Highly Selective Electrocatalytic Reduction of CO$_2$ into Methane on Cu−Bi Nanoalloys

Zhijiang Wang,* Qi Yuan, Jingjing Shan, Zhaohua Jiang, Ping Xu, Yongfeng Hu, Jigang Zhou, Lina Wu, Zhuangzhuang Niu, Jianmin Sun,* Tao Cheng,* and William A. Goddard, III*

ACCESS | Metrics & More | Article Recommendations | Supporting Information

ABSTRACT: Methane (CH$_4$), the main component of natural gas, is one of the most valuable products facilitating energy storage via electricity conversion. However, the poor selectivity and high overpotential for CH$_4$ formation with metallic Cu catalysts prevent realistic applications. Introducing a second element to tune the electronic state of Cu has been widely used as an effective method to improve catalytic performance, but achieving high selectivity and activity toward CH$_4$ remains challenging. Here, we successfully synthesized Cu−Bi NPs, which exhibit a CH$_4$ Faradaic efficiency (FE) as high as 70.6% at −1.2 V versus reversible hydrogen electrode (RHE). The FE of Cu−Bi NPs has increased by approximately 25-fold compared with that of Cu NPs. DFT calculations showed that alloying Cu with Bi significantly decreases the formation energy of *COH formation, the rate-determining step, which explains the improved performance. Further analysis showed that Cu that has been partially oxidized because of electron withdrawal by Bi is the most possible active site.
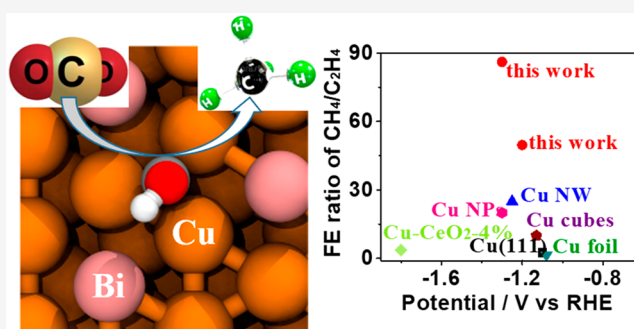
The electrochemical reduction of CO$_2$ into value-added products provides an attractive strategy for reducing atmospheric CO$_2$ concentrations.[1−7] Intensive studies focusing on metal-based electrocatalysts for the CO$_2$ reduction reaction (CO$_2$RR) have been conducted to distinguish candidates that are capable of reducing CO$_2$ into value-added chemicals, such as CO,[8,9] HCOOH,[10,11] CH$_4$,[12,13] C$_2$H$_4$,[14,15] and C$_2$H$_5$OH.[16] Cu is the only pure metal catalyst that is known to electrochemically convert CO$_2$ into appreciable amounts of hydrocarbons, such as CH$_4$ and C$_2$H$_4$. Modifying Cu to achieve high activity and stability with exclusive selectivity for a single class of target hydrocarbons is of great interest.

Considerable progress has been made toward improving catalytic performance in the reduction of CO$_2$ on Cu-based electrodes.[17] The selectivity for the production of C2+ species in CO$_2$RR has been greatly enhanced by tuning the effects of particle size,[18] surface structure,[19] oxidation state,[20] grain boundaries,[21] crystal facets,[22] and components[23] on the performance of Cu electrocatalysts, especially the introduction of Cu$_2$O compositions.[14,15,18,24,25]

Alloying has been proven to be a powerful method for tailoring the electronic properties of metal catalysts; it is based on synergistic effects that can break the scaling relationship to enhance reaction directionality toward a specific hydrocarbon.[26] Various Cu-based binary electrocatalysts, such as Au−Cu,[27] Cu−Pd,[28] and Cu−In alloy,[29] for the CO$_2$RR have been synthesized. These electrodes exhibit improved catalytic performance compared with that of pure metals. CO is the major product of most Cu-based alloys in most cases.[30] Achieving high selectivity for CH$_4$ over Cu is desired but remains a massive challenge.

CH$_4$ is the main component of natural gas and an important energy storage medium with high energy density owing to its high H content (25 wt %). However, the poor selectivity of CH$_4$ production through CO$_2$ reduction prevents its further industrial utilization. The reaction pathway toward CH$_4$ production requires the addition of a proton to the *CO intermediate to generate *CHO or *COH.[31] However, activated protons also tend to combine with each other to produce H$_2$, competing with the formation of CH$_4$. *CO is a quite stable intermediate that requires extensive energy to be protonated. As a result, few catalysts have good selectivity for CH$_4$ production.

Herein, we develop a novel Cu−Bi bimetallic nanocatalyst that presents high efficiency and selective activity for the electrochemical reduction of CO$_2$ into CH$_4$. Charge transfer occurs within Cu and Bi elements such that the Cu in Cu−Bi is promoted to the Cu^{1+} valence state. The electronic property
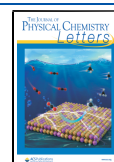
and CO_2RR performance of the Cu^{1+} in Cu−Bi are significantly different from those of the Cu^{1+} in Cu_2O. This feature accounts for the 25-fold enhancement in the ratio of CH_4 to the competing C_2H_4 products shown by the Cu−Bi nanoalloy compared with that exhibited by pure Cu. This ratio is the highest among currently reported Cu-based CO_2RR catalysts.

Cu−Bi bimetallic nanoparticles (NPs) were prepared through a facile one-step method by using copper nitrate and bismuth nitrate as precursors and sodium borohydride as the reductant (see the Supporting Information for experimental details). Transmission electron microscopy (TEM) images show that the as-synthesized Cu−Bi NPs have a core diameter of approximately 5 nm and interconnected dendritic morphologies (Figures 1 and S1−S5). Cu−Bi NPs with similar
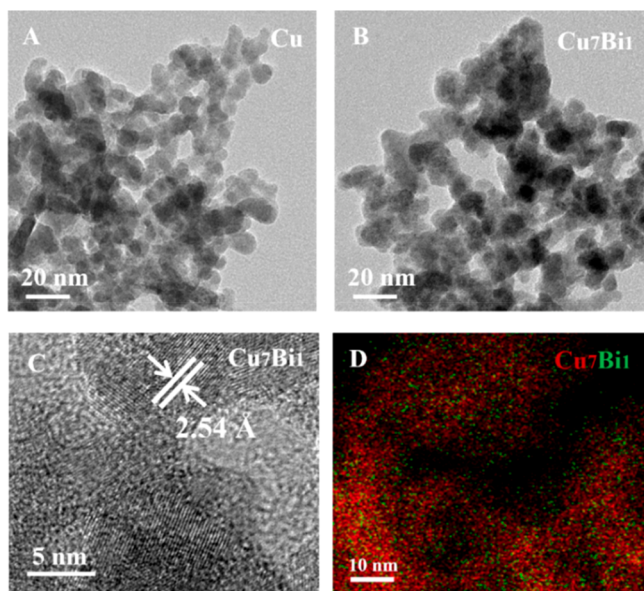
Figure 1. Morphology characterization of Cu and Cu_7Bi_1 NPs. TEM image of (A) Cu and (B) Cu_7Bi_1 NPs; (C) HRTEM image and (D) EDX mapping of Cu_7Bi_1 NPs.

morphologies and particle sizes can be prepared with various stoichiometric ratios (Cu, Cu_9Bi_1, Cu_7Bi_1, Cu_3Bi_1, and Bi). Thus, the enhancement in CO_2RR performance cannot be a size effect. The results of energy-dispersive X-ray spectroscopy elemental analysis for Cu_7Bi_1 NPs (Figure 1D) show that the distribution ranges for Cu (red) and Bi (green) almost completely overlap. This close correlation indicates that Cu and Bi atoms mix randomly within the alloy NPs, forming a solid solution structure. This feature is consistent with the Cu−Bi phase diagram obtained at room temperature. The absence of characteristic Bi peaks in the X-ray diffraction (XRD) patterns of the Cu−Bi NPs (Figure S6) further confirms the formation of a solid solution wherein Bi atoms are distributed within the Cu matrix. HRTEM images (Figures S1−S5) and XRD patterns (Figure S6) show that the lattice distance shifts to a high value as the amount of Bi is increased. This shift can be attributed to the enhanced amount of Bi within the Cu matrix. Meanwhile, the XRD peaks of the synthesized samples exhibit broad bandwidth and low intensity, indicating that the samples have very small particle sizes, in agreement with TEM observations.

The electronic structure of heterogeneous catalysts plays a key role in their catalytic activity. To understand the electronic structure of Cu-based electrocatalysts, we performed X-ray absorption spectroscopy (XAS). Figure 2A shows the Cu K-
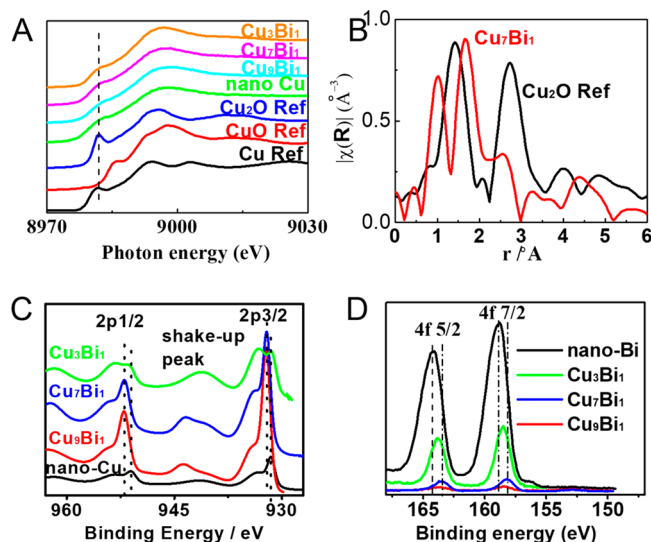
Figure 2. Characterization of the chemical state for the catalysts. (A) Cu K-edge XANES spectra and (B) Cu FT-EXAFS spectra of samples; (C) Cu 2p and (D) Bi 4f XPS spectra of samples.

edge X-ray absorption near-edge structural (XANES) spectra of Cu, Cu_9Bi_1, Cu_7Bi_1, Cu_3Bi_1, and Bi NPs. Comparison with the Cu reference spectra clearly indicates that the Cu in these samples is different from CuO and is similar to reduced Cu, such as metallic Cu and Cu_2O, and likely has partial +1 oxidation character. Through the close comparison of the "white-line" feature of Cu XANES spectra (Figure S7A), the white-line area can be integrated and used to estimate the charge of Cu, as shown in Figure S7B. The peak area of all Cu−Bi NPs is relatively higher than that of the nano-Cu, indicating the presence of a slightly oxidized Cu state in the Cu−Bi NPs. With the increase in the Bi fraction, the peak area increases in the alloys, indicating the transfer of charge from Cu to Bi at the atomic scale.[8,32−34]

The k^3-weighted and Fourier transformed extended X-ray absorption fine structure (EXAFS) spectra of the Cu_7Bi_1 NPs and Cu_2O reference are presented in Figure 2B. The peak of 1.42 Å is assigned to Cu−O interaction. The peak of 2.72 Å is attributed to Cu−Cu interaction.[35] The Cu FT-EXAFS feature of Cu_7Bi_1 NPs is different from that of the Cu_2O reference, suggesting that the alloying of Bi with Cu has affected Cu−O and Cu−Cu interactions. The Cu 2p X-ray photoemission spectroscopy (XPS) peaks in Figure 2C show the peaks locating at 931.5 and 951.0 eV for Cu NPs are shifted to the higher energy of 932.2 and 952.1 eV for Cu_7Bi_1 nanoalloys, respectively. This feature confirms the oxidized state of Cu upon the alloying of Bi with Cu and is in agreement with the Cu XAS results. In Figure 2D, the Bi 4f peaks for Cu−Bi alloys shift to a lower energy compared with those for nano-Bi, with the Bi 4f of Cu_7Bi_1 NPs at the lowest binding energy. Taking the XAS and XPS results together, we conclude that a strong interaction exists between Cu and Bi within Cu−Bi NPs. In this interaction, electrons are donated from Cu to Bi within the Cu−Bi nanoalloy, leading to a Cu^{1+} valence feature.

The CO_2 reduction activities of Cu–Bi NPs with various Cu/Bi atomic ratios were determined by performing constant potential electrolysis in 0.5 M $KHCO_3$ electrolyte saturated with CO_2. The Cu and Cu–Bi NPs reduce CO_2 into multiple products, including CH_4, C_2H_4, CO, and HCOOH (Figure S8). Bi NPs convert CO_2 into HCOOH and CO. All these processes are accompanied by the competing hydrogen evolution reaction (HER).

The Cu alloyed with Bi sharply increases CH_4 selectivity and activity with the following notable observations:

- As-synthesized Cu NPs produce CH_4 with an onset potential of −0.7 V versus the reversible hydrogen electrode (RHE, hereafter all the potentials mentioned are referenced to RHE) and reach a peak Faradaic efficiency (FE) of 20.7% at −1.2 V (Figure 3A).
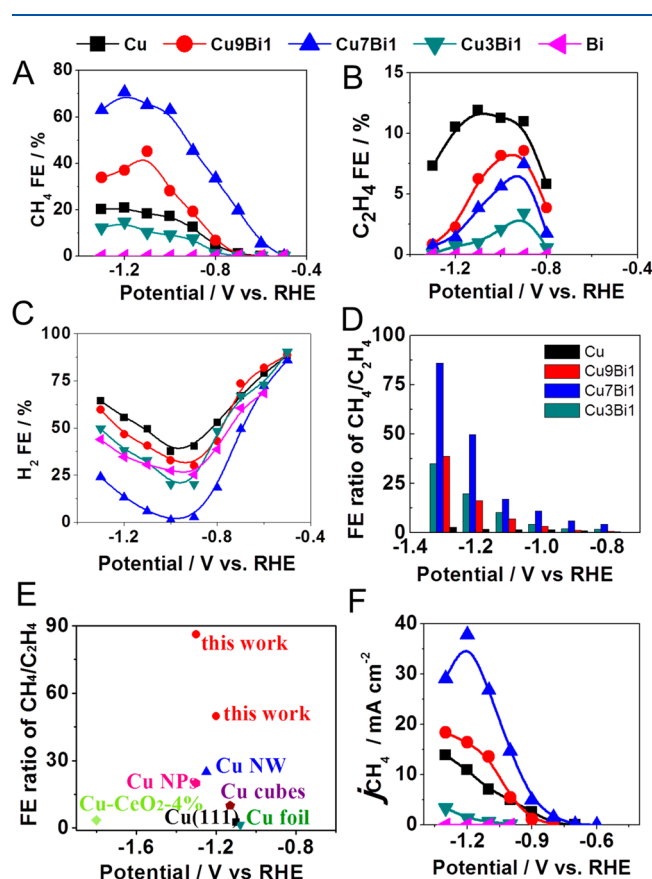
Figure 3. CO_2 electroreduction performance of the synthesized NPs. (A) FE of CH_4, (B) FE of C_2H_4, (C) FE of H_2, (D) FE ratio of CH_4/C_2H_4, (E) comparison on the CH_4 selectivity of current work with prior reports, and (F) CH_4 partial current densities.

- Cu_9Bi_1 NPs yield a peak CH_4 FE of 45.1% at −1.2 V.
- For Cu_7Bi_1 NPs, the maximum CH_4 FE reaches 70.6% at −1.2 V.
- The selectivity for CH_4 formation decreases with further increases in the amounts of Bi in the Cu–Bi alloy, such as Cu_3Bi_1, leading to the FE of 14.7% at the potential of −1.2 V.

Among the Cu–Bi NPs, Cu_7Bi_1 NPs have the lowest onset potential at −0.6 V. C_2H_4 yield is also sensitive to the amount of Bi in the alloy (Figure 3B). The increased amount of Bi in the alloy decreases the production of C_2H_4. The alloying of Bi with Cu is also beneficial for reducing H formation. The

Cu_7Bi_1 NPs have the best performance for suppressing the HER (Figure 3C). Figure 3D shows the FE ratios of CH_4/C_2H_4 at various applied potentials for four kinds of Cu–Bi NPs. Compared with pure Cu NPs, all Cu–Bi NPs show very high selectivity for CH_4 formation. Compared with that of pure Cu NPs, the selectivity of Cu_7Bi_1 NPs is enhanced 25-fold in terms of the ratio of CH_4 to competing C_2H_4 at the applied potential of −1.2 V and is far higher than that of previously reported Cu-based catalysts, such as Cu nanowires,[36] Cu cubes,[37] Cu NPs,[38] Cu-CeO$_2$,[39] and Cu(111)[40] (Figure 3E).

The CH_4 partial current densities (j_{CH_4}) of different NPs are shown in Figure 3F. The Cu_7Bi_1 NPs possess the highest j_{CH_4} over the applied cathode potential range of −0.6 to −1.3 V. Its j_{CH_4} reaches 37.8 mA/cm^2 at −1.2 V. By contrast, the j_{CH_4} of pure Cu NPs is 9.5 mA/cm^2 at −1.2 V. Thus, the CH_4 partial current densities of Cu_7Bi_1 NPs has increased by 4-fold relative to that of sole Cu. As shown in Figure S9, the Cu_7Bi_1 NPs also present significantly improved stability compared with Cu NPs. The alloying of Bi with Cu dramatically prolongs the lifetime of Cu-based catalysts.

We carried out density functional theory (DFT) calculations to investigate the reaction mechanism of CO_2 reduction on Cu and Cu_7Bi_1 NPs by calculating the formation energy of key intermediates. Cu(111) was utilized to simulate Cu NPs. Cu_7Bi_1 (111) was constructed by replacing one Cu with Bi in the Cu primitive cell and used to simulate Cu_7Bi_1 NPs (additional details regarding the simulation models are presented in the Supporting Information). Our previous work[41] indicates that either *COH formation or *CHO formation is the potential rate-determining step that is dependent on the Cu facet. The formation energy of *COH (ΔE_{*COH}) is

$$\Delta E_{*COH} = E_{*COH} - (E_{*CO} + 0.5E_{H_2}) \tag{1}$$

The formation energy of *CHO(ΔE_{*CHO}) is

$$\Delta E_{*COH} = E_{*CHO} - (E_{*CO} + 0.5E_{H_2}) \tag{2}$$

Here, E_{*COH}, E_{*CHO}, and E_{*CO} are the potential energies of *COH, *CHO, and *CO predicted from DFT calculations, respectively. In our calculations, we found that the formation energy of *CHO on Cu_7Bi_1 is 0.81 eV, the formation energy of *CO is −0.09 eV, and the formation energy of *COH is 0.77 eV. Therefore, the formation energy of *COH is 0.04 eV lower than that of *CHO, indicating that *COH is highly likely to be the first reduction product on Cu_7Bi_1 NPs. Meanwhile, we carried out free-energy calculations to predict the reaction barriers and found that the free-energy barrier of *COH formation is 0.89 eV while the free-energy barrier of *CHO formation is 1.02 eV. Therefore, we concluded that the formation of *CHO is kinetically blocked. The optimized atomic structures of *COH on Cu_7Bi_1 NPs and Cu NPs are shown in Figure 4A–D.

We also investigated the formation energies of *CHOH, *CH, *CH$_2$, and *CH$_3$, which are essential reactive intermediates of CH_4 formation. All the formation energies of these products are less than 0.77 eV, indicating that *COH formation is the potential determining step (PDS) in CH_4 formation on Cu_7Bi_1 NPs. The complete reaction pathway of CH_4 formation is provided in the Supporting Information. We also calculated that the formation energy of *COH on Cu is 1.03 eV. This value is consistent with our previously reported
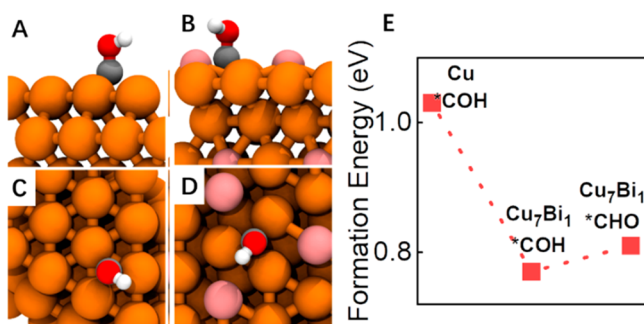
Figure 4. Optimized atomic structures of *COH on Cu from side view (A) and top view (C), on Cu_7Bi_1 from side view (B) and top view (D); (E) formation energy of *COH (in eV) of Cu and Cu_7Bi_1 and *CHO on Cu_7Bi_1. The colors are Cu in orange, C in gray, O in red, and H in white.

value. Thus, introducing Bi into Cu does not change the reaction mechanism but significantly decreases the formation energy of *COH, which determines PDS. This effect explains the experimental observations indicating that Cu_7Bi_1 NPs exhibit improved performance in CO_2RR into CH_4. Lowdin population analysis shows a 0.13 e^- transfer from Cu to Bi that dramatically influences the chemical binding of this intermediate to the catalyst surface. This result is consistent with the results of the above XAS analysis.

C2 formation potentially competes with C1 formation. Thus, we also consider the formation energy of *OC−COH, the widely accepted potential-determining step of C2 formation, in our simulation. Our prediction showed that the formation energy of *OC−COH is 0.91 eV, very close to the previous predictions of 0.95 eV. Considering that the formation energy of *COH is 0.77 eV, it is likely that CO can be directly reduced to CH_4 instead of waiting for another CO to couple to form a C2 product. Our prediction is consistent with experimental observations. Meanwhile, the surface net charge and hydrogen bond (HB) network have been demonstrated to have influence on the DFT predications.[42,43] We have included the solvation effect and HB by including both the implicit solvation model and one explicit water, which represents the minimal simulation model with both effects of the hydrogen bond network. Our simulation results show that the formation energy for *CO to *COH is 0.605 eV in all with one explicit water and implicit solvation model. Thus, with consideration of solvation and HB interaction, the formation of *COH is further stabilized by 0.165 eV, making the CH_4 formation through *COH more favorable, which is consistent with the gas-phase prediction.

In summary, we successfully synthesized a Cu−Bi bimetallic nanocatalyst with improved activity and selectivity for the electrochemical transformation of CO_2 into CH_4. Compared with pure Cu NPs, the Cu_7Bi_1 NPs show selectivity at −1.2 V for CH_4 over C_2H_4 that has been enhanced by 25-fold and CH_4 partial current densities that have been enhanced by 4-fold. DFT calculations suggested that introducing Bi significantly decreases the formation energy of the PDS of CO_2 into CH_4. This effect explains the improvement in CH_4 activity and selectivity. Further analysis demonstrated that the highly electropositive Bi withdraws an electron from Cu, resulting in partially oxidized Cu, which is the most likely active site for CO_2RR into CH_4. These results provide insight into the rational design of efficient Cu-based alloy catalysts for the conversion of CO_2 into specific products.

■ ASSOCIATED CONTENT

ⓢ Supporting Information

The Supporting Information is available free of charge at https://pubs.acs.org/doi/10.1021/acs.jpclett.0c01261.

Experimental procedures and supporting figures (PDF)

■ AUTHOR INFORMATION

Corresponding Authors

Zhijiang Wang − *MIIT Key Laboratory of Critical Materials Technology for New Energy Conversion and Storage and State Key Laboratory of Urban Water Resource and Environment, School of Chemistry and Chemical Engineering, Harbin Institute of Technology, Harbin 150001, China;* ⓞ orcid.org/0000-0001-9314-7922; Email: wangzhijiang@hit.edu.cn

Jianmin Sun − *MIIT Key Laboratory of Critical Materials Technology for New Energy Conversion and Storage, Harbin Institute of Technology, Harbin 150001, China;* ⓞ orcid.org/0000-0002-6682-7479; Email: sunjm@hit.edu.cn

Tao Cheng − *Institute of Functional Nano & Soft Materials (FUNSOM) Jiangsu Key Laboratory for Carbon Based Functional Materials & Devices, Soochow University, Suzhou, Jiangsu 215123, China; Materials and Process Simulation Center (MSC) and Joint Center for Artificial Photosynthesis (JCAP), California Institute of Technology, Pasadena, California 91125, United States;* ⓞ orcid.org/0000-0003-4830-177X; Email: tcheng@caltech.edu

William A. Goddard, III − *Materials and Process Simulation Center (MSC) and Joint Center for Artificial Photosynthesis (JCAP), California Institute of Technology, Pasadena, California 91125, United States;* ⓞ orcid.org/0000-0003-0097-5716; Email: wag@wag.caltech.edu

Authors

Qi Yuan − *Institute of Functional Nano & Soft Materials (FUNSOM) Jiangsu Key Laboratory for Carbon Based Functional Materials & Devices, Soochow University, Suzhou, Jiangsu 215123, China*

Jingjing Shan − *MIIT Key Laboratory of Critical Materials Technology for New Energy Conversion and Storage, Harbin Institute of Technology, Harbin 150001, China*

Zhaohua Jiang − *MIIT Key Laboratory of Critical Materials Technology for New Energy Conversion and Storage and State Key Laboratory of Urban Water Resource and Environment, School of Chemistry and Chemical Engineering, Harbin Institute of Technology, Harbin 150001, China*

Ping Xu − *MIIT Key Laboratory of Critical Materials Technology for New Energy Conversion and Storage, Harbin Institute of Technology, Harbin 150001, China;* ⓞ orcid.org/0000-0002-1516-4986

Yongfeng Hu − *Canadian Light Source Inc., Saskatoon, Saskatchewan S7N 0X4, Canada*

Jigang Zhou − *Canadian Light Source Inc., Saskatoon, Saskatchewan S7N 0X4, Canada;* ⓞ orcid.org/0000-0001-6644-2862

Lina Wu − *Department of Radiology, Molecular Imaging Research Center of Harbin Medical University, the Fourth Hospital of Harbin Medical University, Harbin 150001, China;* ⓞ orcid.org/0000-0002-7517-3606

Zhuangzhuang Niu − *MIIT Key Laboratory of Critical Materials Technology for New Energy Conversion and Storage, Harbin Institute of Technology, Harbin 150001, China*

Complete contact information is available at:

https://pubs.acs.org/10.1021/acs.jpclett.0c01261

Notes

The authors declare no competing financial interest.

■ REFERENCES

(1) Goeppert, A.; Czaun, M.; Jones, J. P.; Prakash, G. S.; Olah, G. A. Recycling of carbon dioxide to methanol and derived products—closing the loop. *Chem. Soc. Rev.* **2014**, *43*, 7995−8048.

(2) Olah, G. A.; Prakash, G. K. S.; Goeppert, A. Anthropogenic Chemical Carbon Cycle for a Sustainable Future. *J. Am. Chem. Soc.* **2011**, *133*, 12881−12898.

(3) Montoya, J. H.; Seitz, L. C.; Chakthranont, P.; Vojvodic, A.; Jaramillo, T. F.; Norskov, J. K. Materials for solar fuels and chemicals. *Nat. Mater.* **2017**, *16*, 70−81.

(4) Rosen, B. A.; Salehi-Khojin, A.; Thorson, M. R.; Zhu, W.; Whipple, D. T.; Kenis, P. J. A.; Masel, R. I. Ionic Liquid-Mediated Selective Conversion of CO_2 to CO at Low Overpotentials. *Science* **2011**, *334*, 643−644.

(5) Wang, Z.; Wu, L.; Sun, K.; Chen, T.; Jiang, Z.; Cheng, T.; Goddard, W. A. Surface Ligand Promotion of Carbon Dioxide Reduction through Stabilizing Chemisorbed Reactive Intermediates. *J. Phys. Chem. Lett.* **2018**, *9*, 3057−3061.

(6) Mistry, H.; Varela, A. S.; Kuehl, S.; Strasser, P.; Cuenya, B. R. Nanostructured electrocatalysts with tunable activity and selectivity. *Nat. Rev. Mater.* **2016**, *1*, 16009.

(7) Liu, M.; Pang, Y.; Zhang, B.; De Luna, P.; Voznyy, O.; Xu, J.; Zheng, X.; Dinh, C. T.; Fan, F.; Cao, C.; de Arquer, F. P. G.; Safaei, T. S.; Mepham, A.; Klinkova, A.; Kumacheva, E.; Filleter, T.; Sinton, D.; Kelley, S. O.; Sargent, E. H. Enhanced electrocatalytic CO_2 reduction via field-induced reagent concentration. *Nature* **2016**, *537*, 382−386.

(8) Sun, K.; Wu, L.; Qin, W.; Zhou, J.; Hu, Y.; Jiang, Z.; Shen, B.; Wang, Z. Enhanced electrochemical reduction of CO_2 to CO on Ag electrocatalysts with increased unoccupied density of states. *J. Mater. Chem. A* **2016**, *4*, 12616−12623.

(9) Wang, Z.; Sun, K.; Liang, C.; Wu, L.; Niu, Z.; Gao, J. Synergistic Chemisorbing and Electronic Effects for Efficient CO_2 Reduction Using Cysteamine-Functionalized Gold Nanoparticles. *ACS Appl. Energy Mater.* **2019**, *2*, 192−195.

(10) Gao, S.; Lin, Y.; Jiao, X.; Sun, Y.; Luo, Q.; Zhang, W.; Li, D.; Yang, J.; Xie, Y. Partially oxidized atomic cobalt layers for carbon dioxide electroreduction to liquid fuel. *Nature* **2016**, *529*, 68−71.

(11) Chen, Y.; Kanan, M. W. Tin oxide dependence of the CO_2 reduction efficiency on tin electrodes and enhanced activity for tin/tin oxide thin-film catalysts. *J. Am. Chem. Soc.* **2012**, *134*, 1986−1989.

(12) Manthiram, K.; Beberwyck, B. J.; Alivisatos, A. P. Enhanced Electrochemical Methanation of Carbon Dioxide with a Dispersible Nanoscale Copper Catalyst. *J. Am. Chem. Soc.* **2014**, *136*, 13319−13325.

(13) Kuhl, K. P.; Hatsukade, T.; Cave, E. R.; Abram, D. N.; Kibsgaard, J.; Jaramillo, T. F. Electrocatalytic Conversion of Carbon Dioxide to Methane and Methanol on Transition Metal Surfaces. *J. Am. Chem. Soc.* **2014**, *136*, 14107−14113.

(14) Mistry, H.; Varela, A. S.; Bonifacio, C. S.; Zegkinoglou, I.; Sinev, I.; Choi, Y. W.; Kisslinger, K.; Stach, E. A.; Yang, J. C.; Strasser, P.; Roldan, B.; et al. Highly selective plasma-activated copper catalysts for carbon dioxide reduction to ethylene. *Nat. Commun.* **2016**, *7*, 12123.

(15) Liang, Z. Q.; Zhuang, T. T.; Seifitokaldani, A.; Li, J.; Huang, C. W.; Tan, C. S.; Li, Y.; De Luna, P.; Dinh, C. T.; Hu, Y.; Xiao, Q.; Hsieh, P. L.; Wang, Y.; Li, F.; Quintero-Bermudez, R.; Zhou, Y.; Chen, P.; Pang, Y.; Lo, S. C.; Chen, L. J.; Tan, H.; Xu, Z.; Zhao, S.; Sinton, D.; Sargent, E. H. Copper-on-nitride enhances the stable electrosynthesis of multi-carbon products from CO_2. *Nat. Commun.* **2018**, *9*, 3828.

(16) Morales-Guio, C. G.; Cave, E. R.; Nitopi, S. A.; Feaster, J. T.; Wang, L.; Kuhl, K. P.; Jackson, A.; Johnson, N. C.; Abram, D. N.; Hatsukade, T.; et al. Improved CO_2 reduction activity towards C2+ alcohols on a tandem gold on copper electrocatalyst. *Nat. Catal.* **2018**, *1*, 764.

(17) Aran-Ais, R. M.; Gao, D.; Cuenya, B. R. Structure- and Electrolyte-Sensitivity in CO_2 Electroreduction. *Acc. Chem. Res.* **2018**, *51*, 2906−2917.

(18) De Luna, P.; Quintero-Bermudez, R.; Dinh, C. T.; Ross, M. B.; Bushuyev, O. S.; Todorović, P.; Regier, T.; Kelley, S. O.; Yang, P.; Sargent, E. H. Catalyst electro-redeposition controls morphology and oxidation state for selective carbon dioxide reduction. *Nat. Catal.* **2018**, *1*, 103.

(19) Li, C. W.; Kanan, M. W. CO_2 reduction at low overpotential on Cu electrodes resulting from the reduction of thick Cu_2O films. *J. Am. Chem. Soc.* **2012**, *134*, 7231−7234.

(20) Ren, D.; Deng, Y.; Handoko, A. D.; Chen, C. S.; Malkhandi, S.; Yeo, B. S. Selective electrochemical reduction of carbon dioxide to ethylene and ethanol on copper (I) oxide catalysts. *ACS Catal.* **2015**, *5*, 2814−2821.

(21) Li, C. W.; Ciston, J.; Kanan, M. W. Electroreduction of carbon monoxide to liquid fuel on oxide-derived nanocrystalline copper. *Nature* **2014**, *508*, 504.

(22) Cheng, T.; Xiao, H.; Goddard, W. A. Reaction mechanisms for the electrochemical reduction of CO_2 to CO and formate on the Cu (100) surface at 298 K from quantum mechanics free energy calculations with explicit water. *J. Am. Chem. Soc.* **2016**, *138*, 13802−13805.

(23) Verdaguer-Casadevall, A.; Li, C. W.; Johansson, T. P.; Scott, S. B.; McKeown, J. T.; Kumar, M.; Stephens, I. E.; Kanan, M. W.; Chorkendorff, I. Probing the active surface sites for CO reduction on oxide-derived copper electrocatalysts. *J. Am. Chem. Soc.* **2015**, *137*, 9808−9811.

(24) Favaro, M.; Xiao, H.; Cheng, T.; Goddard, W. A.; Yano, J.; Crumlin, E. J. Subsurface oxide plays a critical role in CO_2 activation by Cu(111) surfaces to form chemisorbed CO_2, the first step in reduction of CO_2. *Proc. Natl. Acad. Sci. U. S. A.* **2017**, *114*, 6706−6711.

(25) Jung, H.; Lee, S. Y.; Lee, C. W.; Cho, M. K.; Won, D. H.; Kim, C.; Oh, H.-S.; Min, B. K.; Hwang, Y. J. Electrochemical Fragmentation of Cu_2O Nanoparticles Enhancing Selective C−C Coupling from CO_2 Reduction Reaction. *J. Am. Chem. Soc.* **2019**, *141*, 4624−4633.

(26) Peterson, A. A.; Norskov, J. K. Activity Descriptors for CO_2 Electroreduction to Methane on Transition-Metal Catalysts. *J. Phys. Chem. Lett.* **2012**, *3*, 251−258.

(27) Kim, D.; Resasco, J.; Yu, Y.; Asiri, A. M.; Yang, P. Synergistic geometric and electronic effects for electrochemical reduction of carbon dioxide using gold−copper bimetallic nanoparticles. *Nat. Commun.* **2014**, *5*, 4948.

(28) Ma, S.; Sadakiyo, M.; Heima, M.; Luo, R.; Haasch, R. T.; Gold, J. I.; Yamauchi, M.; Kenis, P. J. Electroreduction of carbon dioxide to hydrocarbons using bimetallic Cu−Pd catalysts with different mixing patterns. *J. Am. Chem. Soc.* **2017**, *139*, 47−50.

(29) Rasul, S.; Anjum, D. H.; Jedidi, A.; Minenkov, Y.; Cavallo, L.; Takanabe, K. A highly selective copper−indium bimetallic electro-catalyst for the electrochemical reduction of aqueous CO_2 to CO. *Angew. Chem., Int. Ed.* **2015**, *54*, 2146−2150.

(30) Lee, C. W.; Yang, K. D.; Nam, D. H.; Jang, J. H.; Cho, N. H.; Im, S. W.; Nam, K. T. Defining a Materials Database for the Design of Copper Binary Alloy Catalysts for Electrochemical CO_2 Conversion. *Adv. Mater.* **2018**, *30*, 1704717.

(31) Qiu, Y.; Zhong, H.; Xu, W.; Zhang, T.; Li, X.; Zhang, H. Tuning the electrocatalytic properties of a Cu electrode with organic additives containing amine group for CO_2 reduction. *J. Mater. Chem. A* **2019**, *7*, 5453−5462.

(32) Sun, K.; Cheng, T.; Wu, L.; Hu, Y.; Zhou, J.; Maclennan, A.; Jiang, Z.; Gao, Y.; Goddard, W. A.; Wang, Z. Ultrahigh Mass Activity for Carbon Dioxide Reduction Enabled by Gold−Iron Core−Shell Nanoparticles. *J. Am. Chem. Soc.* **2017**, *139*, 15608−15611.

(33) Bzowski, A.; Sham, T.; Yiu, Y. Ag L-edge x-ray-absorption near-edge-structure study of charge redistribution at the Ag site in Au-Ag alloys. *Phys. Rev. B: Condens. Matter Mater. Phys.* **1994**, *49*, 13776−13779.

(34) Zhang, P.; Zhou, X.; Tang, Y.; Sham, T. K. Organosulfur-Functionalized Au, Pd, and Au−Pd Nanoparticles on 1D Silicon Nanowire Substrates: Preparation and XAFS Studies. *Langmuir* **2005**, *21*, 8502−8508.

(35) Iwasawa, Y.; Asakura, K.; Tada, M. *XAFS Techniques for Catalysts, Nanomaterials, and Surfaces*; Springer, 2017; pp 39−50.

(36) Li, Y.; Cui, F.; Ross, M. B.; Kim, D.; Sun, Y.; Yang, P. Structure-Sensitive CO_2 Electroreduction to Hydrocarbons on Ultrathin 5-fold Twinned Copper Nanowires. *Nano Lett.* **2017**, *17*, 1312−1317.

(37) Grosse, P.; Gao, D. F.; Scholten, F.; Sinev, I.; Mistry, H.; Roldan Cuenya, B. Dynamic Changes in the Structure, Chemical State and Catalytic Selectivity of Cu Nanocubes during CO_2 Electro-reduction: Size and Support Effects. *Angew. Chem., Int. Ed.* **2018**, *57*, 6192−6197.

(38) Lum, Y.; Kwon, Y.; Lobaccaro, P.; Chen, L.; Clark, E. L.; Bell, A. T.; Ager, J. W. Trace Levels of Copper in Carbon Materials Show Significant Electrochemical CO_2 Reduction Activity. *ACS Catal.* **2016**, *6*, 202−209.

(39) Wang, Y.; Chen, Z.; Han, P.; Du, Y.; Gu, Z.; Xu, X.; Zheng, G. Single-Atomic Cu with Multiple Oxygen Vacancies on Ceria for Electrocatalytic CO_2 Reduction to CH_4. *ACS Catal.* **2018**, *8*, 7113−7119.

(40) Huang, Y.; Handoko, A. D.; Hirunsit, P.; Yeo, B. S. Electrochemical Reduction of CO_2 Using Copper Single-Crystal Surfaces: Effects of CO* Coverage on the Selective Formation of Ethylene. *ACS Catal.* **2017**, *7*, 1749−1756.

(41) Cheng, T.; Xiao, H.; Goddard, W. A. Free-Energy Barriers and Reaction Mechanisms for the Electrochemical Reduction of CO on the Cu(100) Surface, Including Multiple Layers of Explicit Solvent at pH 0. *J. Phys. Chem. Lett.* **2015**, *6*, 4767−4773.

(42) Kim, D.; Shi, J.; Liu, Y. Substantial Impact of Charge on Electrochemical Reactions of Two-Dimensional Materials. *J. Am. Chem. Soc.* **2018**, *140*, 9127−9131.

(43) Zhao, X.; Liu, Y. Unveiling the Active Structure of Single Nickel Atom Catalysis: Critical Roles of Charge Capacity and Hydrogen Bonding. *J. Am. Chem. Soc.* **2020**, *142*, 5773−5777.